Computer Assisted Mechanics and Engineering Sciences, **12**: 341–361, 2005.

Nonlinear vibrations of a moving rail-vehicle excited by snaking and lateral impacts of wheel sets

Marian Klasztorny
Institute of Mechanics & Design, Warsaw University of Technology,
ul. Narbutta 85, 02-524 Warsaw, Poland
e-mail: klasz@wip.pw.edu.pl

(Received April 2, 2004)

The paper develops a theory of physically non-linear vibrations of a rail-vehicle moving on a rectilinear and non-deformable track. The vibrations are excited by snaking and lateral impacts of the wheel sets. De Pater's microspin model and a new simplified model of lateral impacts are applied. An algorithm for determining quasi-steady-state vibrations of the vehicle has been formulated and programmed in Pascal. The simulations have been performed for a Shinkansen rail-vehicle moving at service velocities 160–300 km/h.

1. Introduction

Snaking and lateral impacts of wheel sets are principal factors exciting spatial vibrations of a rail-vehicle moving on a rectilinear track. The snaking phenomenon results from conicity of wheel treads. Unstable snake-like motion of wheel sets is limited by a finite clearance between the wheel flange and the rail head. In this case, there occur lateral impacts of wheel flanges onto rail heads. Snaking and lateral impacts phenomena are strongly physically nonlinear. Other factors inducing spatial vibrations of a rail-vehicle include: small asymmetry of rail-vehicle with respect to a vertical plane coinciding the track axis, geometric imperfections of wheels and rails, fluctuations of stiffness parameters of sub-track layers, blasts of wind etc.

In the 50s and 60s of the previous century, simplified models of snaking of wheel sets were applied, among others the harmonic motion model developed by A.N. Nikolskij [1]. Valuable progress contains Ref. [2], in which A. De Pater developed the microspin theory of a wheel set with the conical wheel tread. De Pater assumed Coulomb's kinetic sliding friction and a rectilinear non-deformable track.

V.K. Garg and R.V. Dukkipati [3] presented more exact modelling of the wheel-track contact problem. They developed Hertz's two-curvature theory of longitudinal, lateral and rotational creep of the wheel moving on a rectilinear or horizontally curved track. The writers presented a methodology of determining complex nonlinear equations of motion of a rail-vehicle, according to the second rank theory. However, they did not include any numerical analyses.

J. Kisilowski et al. [4] presented a wide literature review and achievements of the research team from the Institute of Transport, Warsaw University of Technology, in the field of modelling and dynamic analysis of the moving rail-vehicle – track system. The writers presented planar and spatial, discrete and discrete-continuous models of a rail-vehicle, with linear or nonlinear suspensions. Equations of motion that govern vibrations of a rail-vehicle have been derived under an assumption of large rotations of rigid bodies. A number of track models have been considered, including Euler's or Timoshenko's beams resting on Winkler's or Vlasov's foundations. The writers have applied Kalker's empirical microspin theory describing snaking of wheel sets.

In this study, a theory of physically nonlinear vibrations of a rail-vehicle has been developed. Vibrations of the vehicle moving on a rectilinear and non-deformable track are excited by snaking

and lateral impacts of the wheel sets. There are applied de Pater's microspin model and a new simplified model of lateral impacts. An algorithm for determining quasi-steady-state vibrations of the vehicle has been formulated and programmed in Pascal. The simulations have been performed for a Shinkansen rail-vehicle moving at service velocities 160–300 km/h.

2. Modelling snaking of moving wheel sets

A. De Pater [2] formulated the microspin theory for a single moving wheel set. In this paper, de Pater's theory is developed via including dynamic interactions carried by suspensions of a spatially vibrating rail-vehicle.

The following assumptions are made:

- A wheel set is a rigid body with three planes of symmetry.
- A wheel tread is conical and compatible with the inclination of the rail tread.
- The kinetic sliding friction forces are described by Coulomb's model.
- The kinetic sliding friction ratio is constant.
- There is no roughness on wheel and rail treads.
- Separation of the wheel tread from the rail tread is impossible.
- The clearance between the wheel flange and the rail head, measured in the central position of the wheel set, i.e. the nominal clearance, is constant along the track.
- The track is continuous, rectilinear and non-deformable.
- A service velocity $\bar{v}$ of a rail-vehicle is constant.
- The rail-vehicle is stiffly guided in the direction of the track axis.

A moving wheel set in the central position, with respect to the track, is shown in Fig. 1. The wheel and rail treads are inclined at angle γ. Vibrations of the set are described in the inertial

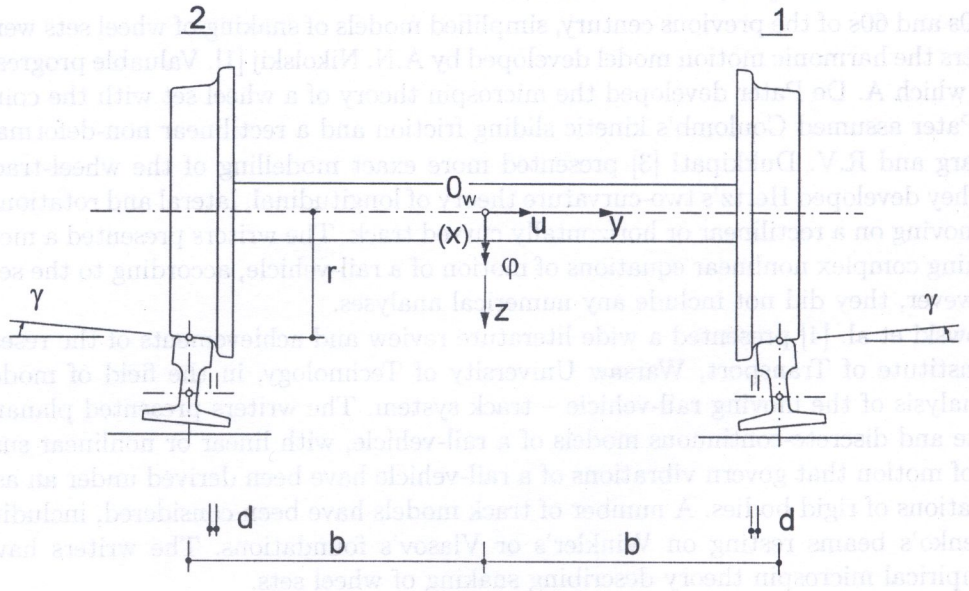

Fig. 1. The central position of the moving wheel set with respect to the rails

system xyz, where axes x, y, z are the principal axes of inertia of the rigid body reflecting the wheel set. According to de Pater's microspin theory a moving wheel set has two degrees of freedom, i.e. $u(t)$ – the lateral translation, $\varphi(t)$ – the angle of snaking. The remaining displacements of the wheel set result from stiff guiding of the vehicle, i.e. a service motion $\bar{v}t$ and a rotational motion about axis y with angular velocity $\bar{v}/r$ where r is a radius of the central tread of the wheel.

Displacements u, φ generate longitudinal and lateral spins of velocities v_x, v_y which induce Coulomb's kinetic sliding friction forces of components F_{x1}, F_{y1} for wheel 1 and F_{x2}, F_{y2} for wheel 2 (see Fig. 2). The schemes that illustrate determination of the longitudinal and lateral sliding velocities are shown in Fig. 3. Displacement u increases the radius of wheel 1 and decreases the radius of wheel 2 by the same value $u \tan\gamma \approx u\gamma$. Applying the superposition rule, one obtains [2]

velocity of longitudinal spin of wheel 1:

$$\bar{v} - \bar{v}(r + u\gamma)/r = -\bar{v}u\gamma/r, \tag{1}$$

velocity of longitudinal spin of wheel 2:

$$\bar{v} - \bar{v}(r - u\gamma)/r = \bar{v}u\gamma/r. \tag{2}$$

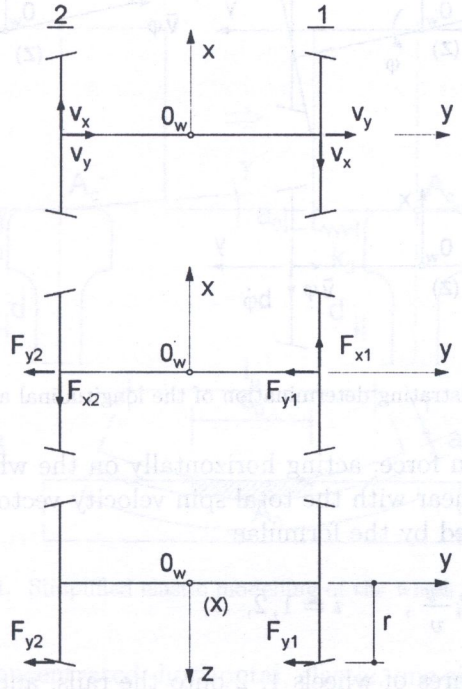

Fig. 2. Longitudinal and lateral spin velocities and sliding friction forces

Snaking angle φ produces lateral spin velocity $-\bar{v}\varphi$ since the vehicle is stiffly guided in the x direction (see Fig. 3e). Taking into account the direct and indirect components of the longitudinal and lateral spin velocities, one obtains

$$v_x = \frac{\bar{v}\gamma}{r}u + b\dot{\varphi}, \qquad v_y = \dot{u} - \bar{v}\varphi, \tag{3}$$

where b is half of the rail base. The total spin velocity of the wheel equals

$$v = \sqrt{v_x^2 + v_y^2}. \tag{4}$$

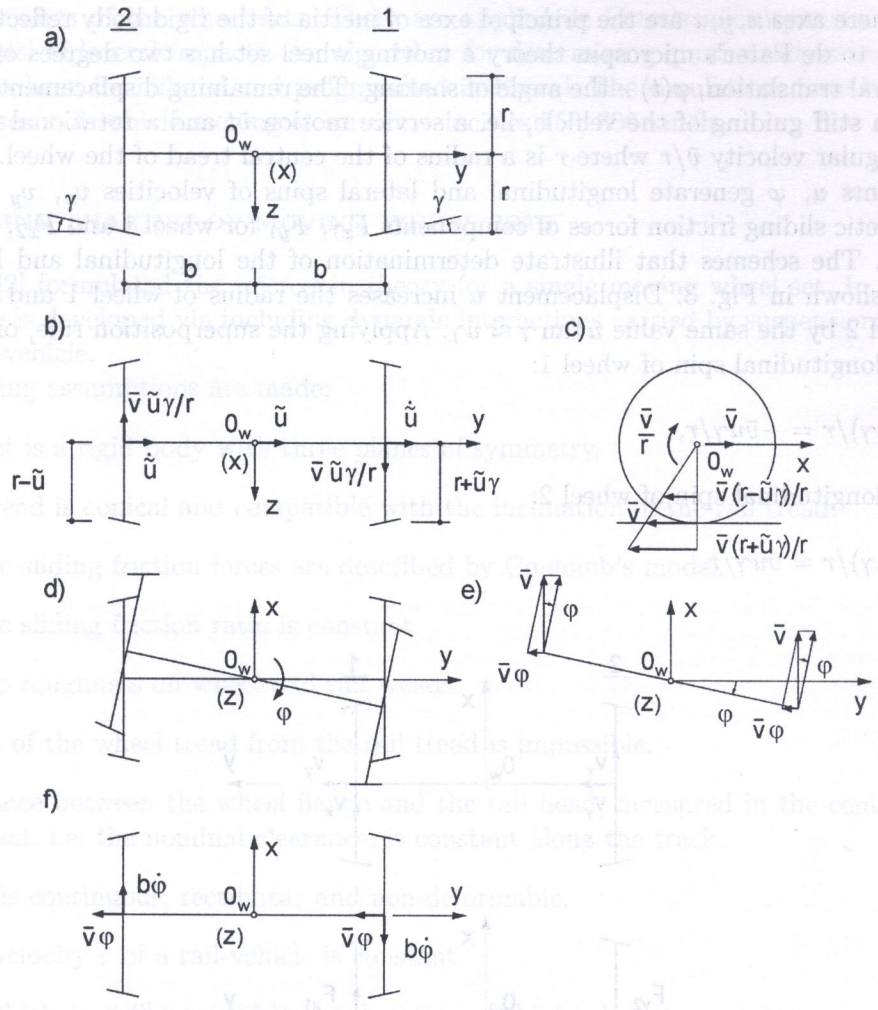

Fig. 3. The schemes illustrating determination of the longitudinal and lateral spin velocities

The Coulomb sliding friction force, acting horizontally on the wheel in the central point of the wheel-rail contact area, is co-linear with the total spin velocity vector. According to Fig. 2, friction forces' components are expressed by the formulae

$$F_{xi} = \mu P_i \frac{v_x}{v}\,, \qquad F_{yi} = \mu P_i \frac{v_y}{v}\,, \qquad i = 1, 2, \tag{5}$$

where P_1, P_2 are vertical pressures of wheels 1, 2 onto the rails, and μ is a wheel-rail kinetic sliding friction ratio. These vertical pressures contain static and dynamic components which will be determined in Sec. 4.

The sliding forces are the wheel-rail interaction forces predicted in the recurrent-iterative loop in numerical integration of the equations of motion [5]. In this case the sliding friction characteristic has to be smoothed. It can be performed with artificial supercritical viscous damping around the singular point [5]. Formulae (5) are then modified to the form ($i = 1, 2$):

$$F_{xi} = \begin{cases} \mu P_i \dfrac{v_x}{v}\,, & v \geq \lambda\,, \\ \mu P_i \dfrac{v_x}{\lambda}\,, & v < \lambda\,, \end{cases} \qquad F_{yi} = \begin{cases} \mu P_i \dfrac{v_y}{v}\,, & v \geq \lambda\,, \\ \mu P_i \dfrac{v_y}{\lambda}\,, & v < \lambda\,, \end{cases} \tag{6}$$

where λ is a smoothing parameter. The value of λ [m/s] is matched from a required accuracy of the simulated processes.

3. Modelling lateral impacts of moving wheel sets

Asymptotically stable or stable snake-like motions of the wheel set protect the condition $|u(t)| < d$ and lateral impacts of wheel flanges onto rail heads do not appear. On the other hand, unstable motion of the wheel set induces those impacts.

In practice, wheel flanges are elastic. A simplified elastic model of the wheel flange can be assumed in the form presented in Fig. 4. Only shear stiffness of the short cantilever is taken into consideration. This cantilever is of length a_o and of rectangular cross-section of dimensions c_o, h_o, where:

- a_o – vertical distance of points A_o, A_c,
- A_o – theoretical point of pressure of the wheel flange onto the rail head,
- A_c – central point of the rail tread,
- c_o – width of the cantilever,
- h_o – thickness of the wheel flange at level A_o.

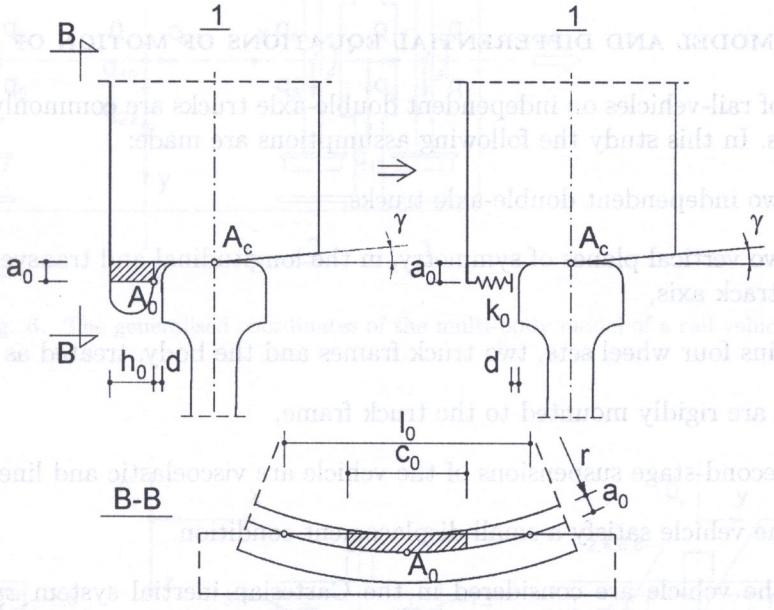

Fig. 4. Simplified elastic modelling of the wheel flange

Stiffness of the equivalent concentrated, horizontal, elastic, one-side constraint equals:

$$k_o = \eta \frac{G c_o h_o}{a_o}, \tag{7}$$

where G is a Kirchhoff's modulus of the wheel flange material, while $\eta \approx 1$ is a corrective coefficient resulting from the real shapes of rail and wheel flanges. Breadth of the cantilever may be assumed to be equal half of the cord l_o, hence

$$c_o = \sqrt{(2r + a_o)a_o}. \tag{8}$$

The horizontal pressures of the wheel flange onto the rail heads, shown in Fig. 5, are calculated from simple formulae

$$P_{h1}(t) = \begin{cases} 0 & , \quad u(t) \le d\,, \\ k_o\,[u(t) - d], & u(t) > d\,, \end{cases} \qquad P_{h2}(t) = \begin{cases} 0 & , \quad u(t) \ge -d\,, \\ -k_o\,[u(t) + d], & u(t) < -d\,. \end{cases} \tag{9}$$

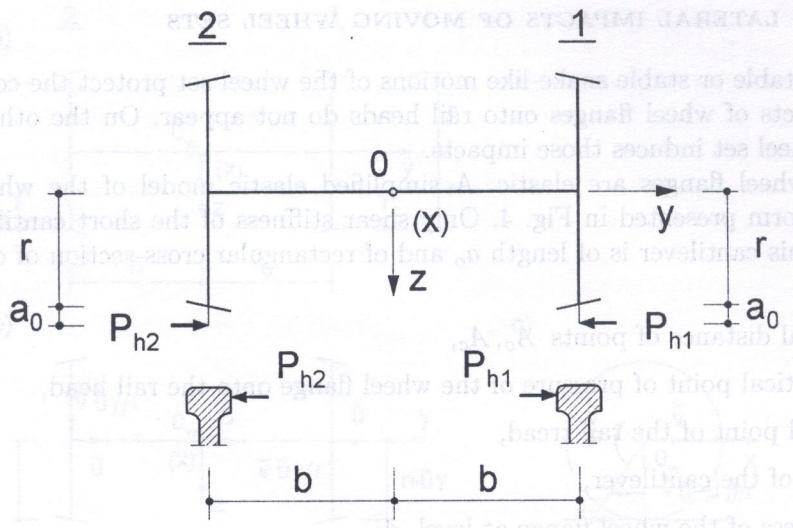

Fig. 5. The horizontal pressures of the wheel flanges onto the rail heads

4. The physic model and differential equations of motion of a rail-vehicle

Trains composed of rail-vehicles on independent double-axle trucks are commonly serviced on high-speed railway lines. In this study the following assumptions are made:

- a vehicle has two independent double-axle trucks,
- a vehicle has two vertical planes of symmetry, in the longitudinal and transverse directions with respect to the track axis,
- a vehicle contains four wheel sets, two truck frames and the body, treated as rigid solids,
- railway motors are rigidly mounted to the truck frame,
- the first- and second-stage suspensions of the vehicle are viscoelastic and linear,
- vibrations of the vehicle satisfy a small displacement condition.

Vibrations of the vehicle are considered in the Cartesian inertial system xyz with the origin coinciding the mass centre of the body (Fig. 6). Axis x is parallel to the track axis, while axes y, z are principal axes of inertia of the body. The rail-vehicle has 23 DOF related to the generalised displacements shown in Fig. 6. Each wheel set has 2 DOF (lateral displacement and snaking angle). Each truck frame or the body has 5 DOF related to lateral displacement, overshooting (vertical displacement), duck-like motion (rotation about axis x), galloping (rotation about axis y) and snaking (rotation about axis z). All displacements are related to mass centres of the vehicle's solids. Vibrations of a moving rail-vehicle are described by vector $\mathbf{q} = \mathrm{col}(q_1, q_2, ..., q_{23})$ of generalised coordinates which are measured from the static equilibrium in the central position of the vehicle on a rectilinear non-deformable track.

The first- and second-stage suspensions are configured as shown in Figs. 7, 8. The rail-vehicle has 20 first-stage suspensions, i.e. 8 vertical translation elements, 8 horizontal translation elements and 4 rotational elements working in the horizontal plane. A system of 10 second-stage suspensions consists of 4 vertical translation elements, 4 horizontal translation elements and 2 rotational elements working in the horizontal plane.

The kinetic energy of the rail-vehicle equals

$$E_k = \frac{1}{2}\dot{\mathbf{q}}^{\mathrm{T}}\mathbf{B}\dot{\mathbf{q}}, \tag{10}$$

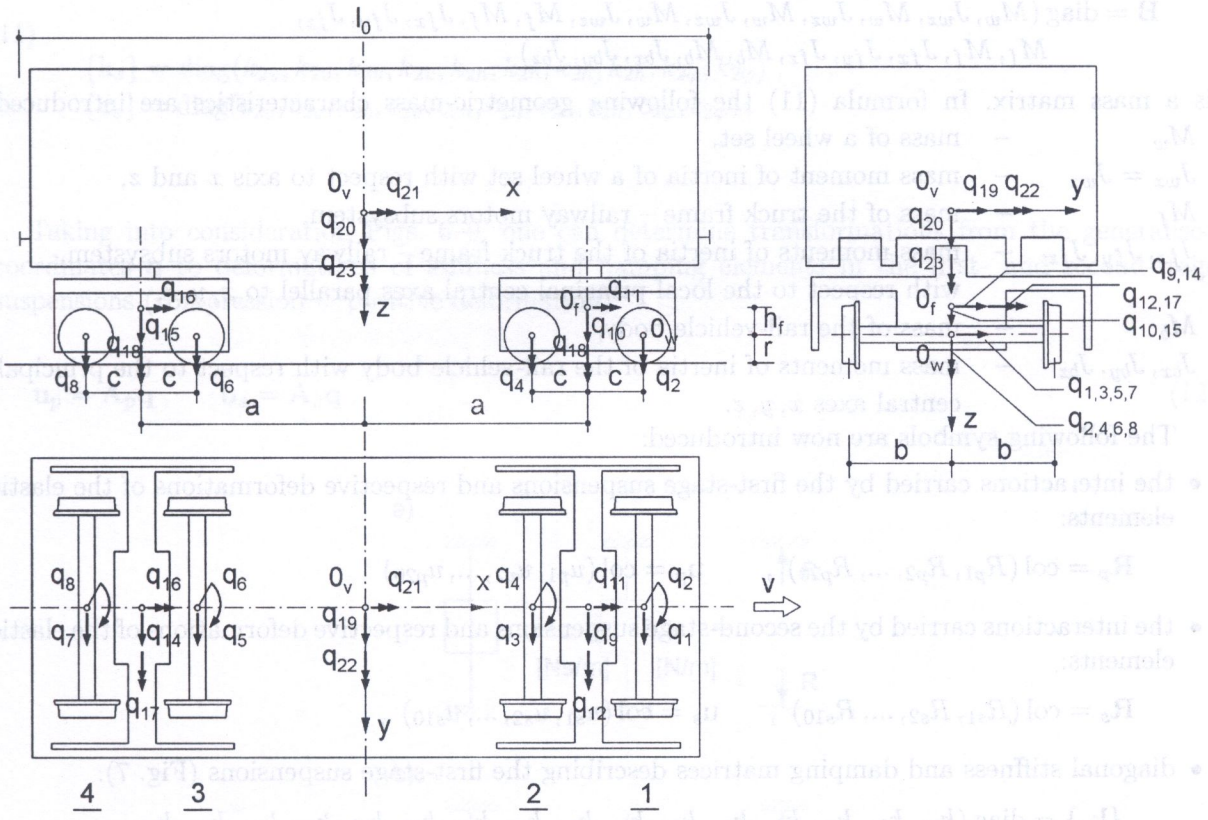

Fig. 6. The generalised coordinates of the multi-body model of a rail-vehicle

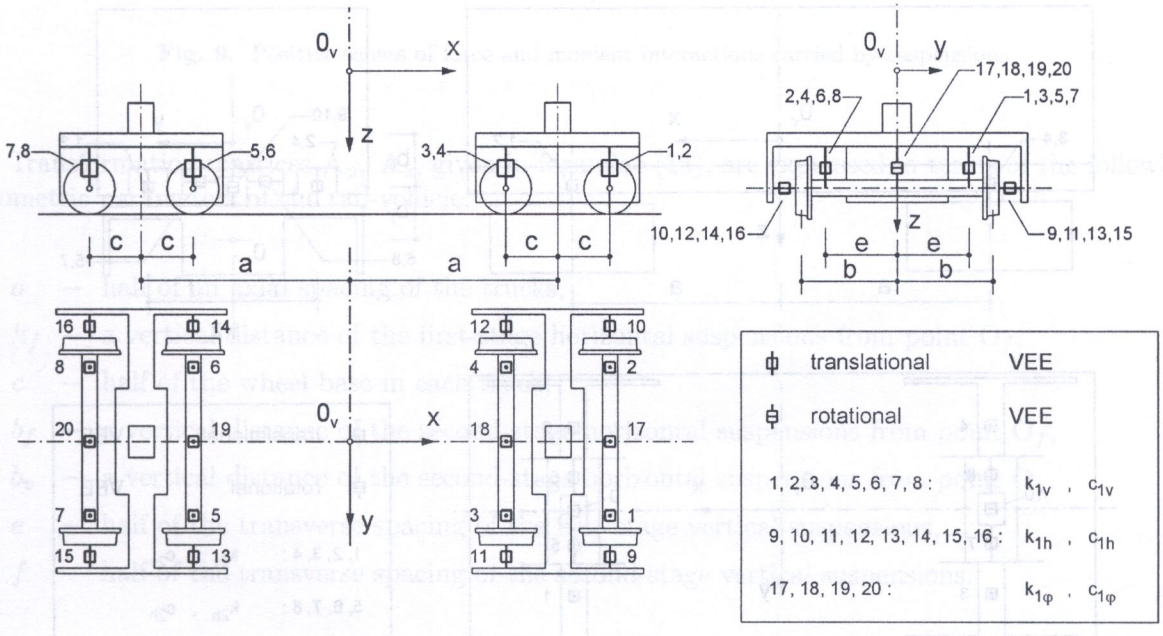

Fig. 7. The first-stage suspensions of a rail-vehicle

where

$$\mathbf{B} = \text{diag}\,(M_w, J_{wz}, M_w, J_{wz}, M_w, J_{wz}, M_w, J_{wz}, M_f, M_f, J_{fx}, J_{fy}, J_{fz}, M_f, M_f, J_{fx}, J_{fy}, J_{fz}, M_b, M_b, J_{bx}, J_{by}, J_{bz}) \tag{11}$$

is a mass matrix. In formula (11) the following geometric-mass characteristics are introduced:

M_w – mass of a wheel set,

$J_{wx} = J_{wz}$ – mass moment of inertia of a wheel set with respect to axis x and z,

M_f – mass of the truck frame – railway motors subsystem,

J_{fx}, J_{fy}, J_{fz} – mass moments of inertia of the truck frame – railway motors subsystem, with respect to the local principal central axes parallel to x, y, z,

M_b – mass of the rail-vehicle body,

J_{bx}, J_{by}, J_{bz} – mass moments of inertia of the rail-vehicle body with respect to the principal central axes x, y, z.

The following symbols are now introduced:

- the interactions carried by the first-stage suspensions and respective deformations of the elastic elements:

$$\mathbf{R}_p = \text{col}\,(R_{p1}, R_{p2}, ..., R_{p20}) \ , \qquad \mathbf{u}_p = \text{col}\,(u_{p1}, u_{p2}, ..., u_{p20}) \ ,$$

- the interactions carried by the second-stage suspensions and respective deformations of the elastic elements:

$$\mathbf{R}_s = \text{col}\,(R_{s1}, R_{s2}, ..., R_{s10}) \ , \qquad \mathbf{u}_s = \text{col}\,(u_{s1}, u_{s2}, ..., u_{s10}) \ ,$$

- diagonal stiffness and damping matrices describing the first-stage suspensions (Fig. 7):

$$\{\mathbf{k}_p\} = \text{diag}\,(k_{1v}, k_{1v}, k_{1v}, k_{1v}, k_{1v}, k_{1v}, k_{1v}, k_{1v}, k_{1h}, k_{1h}, k_{1h}, k_{1h}, k_{1h}, k_{1h}, k_{1h}, k_{1h}, k_{1\varphi}, k_{1\varphi}, k_{1\varphi}, k_{1\varphi}) \ ,$$

$$\{\mathbf{c}_p\} = \text{diag}\,(c_{1v}, c_{1v}, c_{1v}, c_{1v}, c_{1v}, c_{1v}, c_{1v}, c_{1v}, c_{1h}, c_{1h}, c_{1h}, c_{1h}, c_{1h}, c_{1h}, c_{1h}, c_{1h}, c_{1\varphi}, c_{1\varphi}, c_{1\varphi}, c_{1\varphi}) \ ,$$

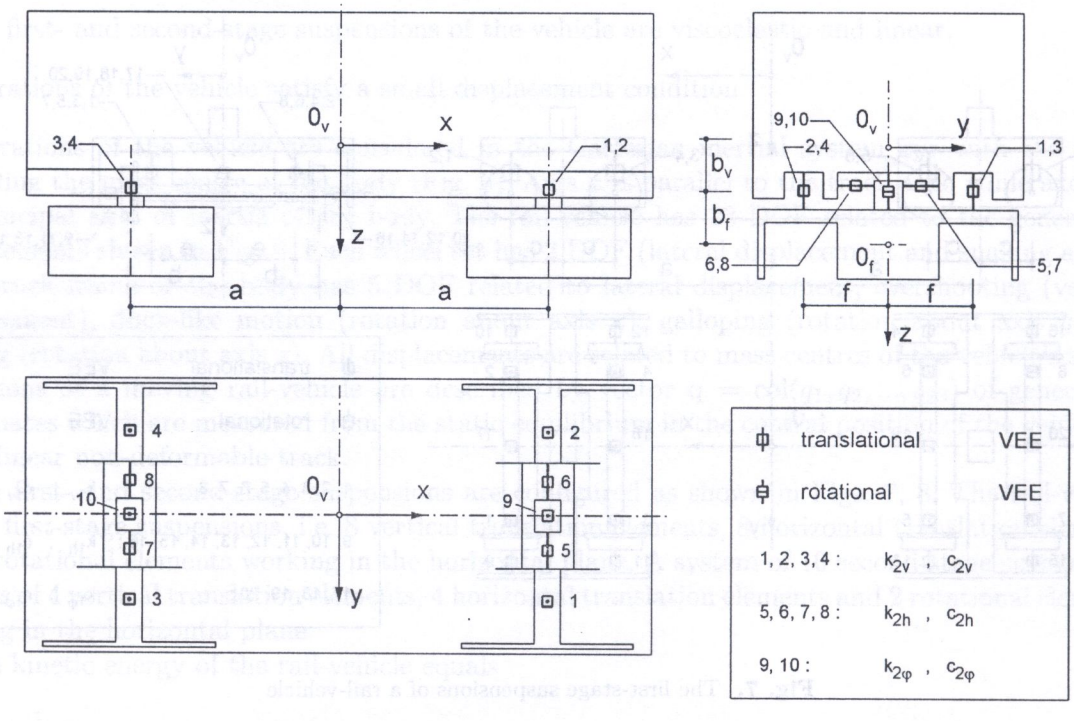

Fig. 8. The second-stage suspensions of a rail-vehicle

- diagonal stiffness and damping matrices describing the second-stage suspensions (Fig. 8):

$$\{\mathbf{k}_s\} = \mathrm{diag}(k_{2v}, k_{2v}, k_{2v}, k_{2v}, k_{2h}, k_{2h}, k_{2h}, k_{2h}, k_{2\varphi}, k_{2\varphi}) ,$$
$$\{\mathbf{c}_s\} = \mathrm{diag}(c_{2v}, c_{2v}, c_{2v}, c_{2v}, c_{2h}, c_{2h}, c_{2h}, c_{2h}, c_{2\varphi}, c_{2\varphi}) .$$

Taking into consideration Figs. 6–9, one can determine transformations from the generalised coordinates $\mathbf{q}$ to deformations of stiffness and damping elements in the first- and second-stage suspensions (compression = positive deformation):

$$\mathbf{u}_p = \mathbf{A}_p\mathbf{q} , \qquad \mathbf{u}_s = \mathbf{A}_s\mathbf{q} . \tag{12}$$

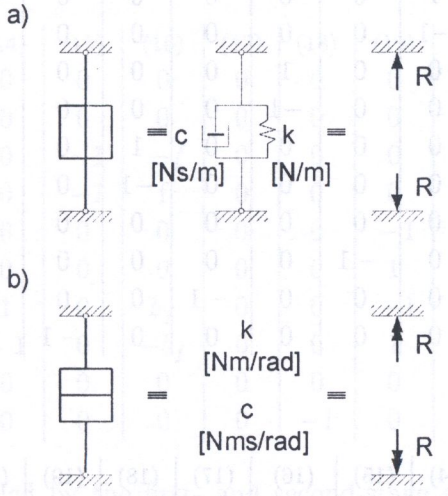

Fig. 9. Positive senses of force and moment interactions carried by suspensions

Transformation matrices $\mathbf{A}_p$, $\mathbf{A}_s$, given in formulae (13), are expressed in terms of the following geometric parameters of the rail-vehicle:

- a – half of an axial spacing of the trucks,
- h_f – a vertical distance of the first-stage horizontal suspensions from point O_f,
- c – half of the wheel base in each truck,
- b_f – a vertical distance of the second-stage horizontal suspensions from point O_f,
- b_v – a vertical distance of the second-stage horizontal suspensions from point O_v,
- e – half of the transverse spacing of the first-stage vertical suspensions,
- f – half of the transverse spacing of the second-stage vertical suspensions.

where O_f, O_v are mass centres of the truck frame – railway motors subsystem and the rail-vehicle body, respectively. In practice, the first-stage vertical suspensions are outside the wheels, i.e. $e > b$. In order to protect clarity in Fig. 6, the symbols of these suspensions are marked between the wheels.

$$\mathbf{A}_p =$$

	(1)	(2)	(3)	(4)	(5)	(6)	(7)	(8)	(9)	(10)	(11)
(1)	0	0	0	0	0	0	0	0	0	1	e
(2)	0	0	0	0	0	0	0	0	0	1	$-e$
(3)	0	0	0	0	0	0	0	0	0	1	e
(4)	0	0	0	0	0	0	0	0	0	1	$-e$
(5)	0	0	0	0	0	0	0	0	0	0	0
(6)	0	0	0	0	0	0	0	0	0	0	0
(7)	0	0	0	0	0	0	0	0	0	0	0
(8)	0	0	0	0	0	0	0	0	0	0	0
(9)	1	0	0	0	0	0	0	0	-1	0	h_f
(10)	-1	0	0	0	0	0	0	0	1	0	$-h_f$
(11)	0	0	1	0	0	0	0	0	-1	0	h_f
(12)	0	0	-1	0	0	0	0	0	1	0	$-h_f$
(13)	0	0	0	0	1	0	0	0	0	0	0
(14)	0	0	0	0	-1	0	0	0	0	0	0
(15)	0	0	0	0	0	0	1	0	0	0	0
(16)	0	0	0	0	0	0	-1	0	0	0	0
(17)	0	-1	0	0	0	0	0	0	0	0	0
(18)	0	0	0	-1	0	0	0	0	0	0	0
(19)	0	0	0	0	0	-1	0	0	0	0	0
(20)	0	0	0	0	0	0	0	-1	0	0	0

	(12)	(13)	(14)	(15)	(16)	(17)	(18)	(19)	(20)	(21)	(22)	(23)
(1)	$-c$	0	0	0	0	0	0	0	0	0	0	0
(2)	$-c$	0	0	0	0	0	0	0	0	0	0	0
(3)	c	0	0	0	0	0	0	0	0	0	0	0
(4)	c	0	0	0	0	0	0	0	0	0	0	0
(5)	0	0	0	1	e	$-c$	0	0	0	0	0	0
(6)	0	0	0	1	$-e$	$-c$	0	0	0	0	0	0
(7)	0	0	0	1	e	c	0	0	0	0	0	0
(8)	0	0	0	1	$-e$	c	0	0	0	0	0	0
(9)	0	$-c$	0	0	0	0	0	0	0	0	0	0
(10)	0	c	0	0	0	0	0	0	0	0	0	0
(11)	0	c	0	0	0	0	0	0	0	0	0	0
(12)	0	$-c$	0	0	0	0	0	0	0	0	0	0
(13)	0	0	-1	0	h_f	0	0	0	0	0	0	0
(14)	0	0	1	0	$-h_f$	0	0	0	0	0	0	0
(15)	0	0	-1	0	h_f	0	0	0	0	0	0	0
(16)	0	0	1	0	$-h_f$	0	0	0	0	0	0	0
(17)	0	1	0	0	0	0	0	0	0	0	0	0
(18)	0	1	0	0	0	0	0	0	0	0	0	0
(19)	0	0	0	0	0	0	0	0	0	0	0	0
(20)	0	0	0	0	0	0	0	0	0	0	0	0

(13)

$$\mathbf{A}_s = \begin{array}{c|cccccccccc} & (1) & (2) & (3) & (4) & (5) & (6) & (7) & (8) & (9) & (10) \\ \hline (1) & 0 & 0 & 0 & 0 & 0 & 0 & 0 & 0 & 0 & -1 \\ (2) & 0 & 0 & 0 & 0 & 0 & 0 & 0 & 0 & 0 & -1 \\ (3) & 0 & 0 & 0 & 0 & 0 & 0 & 0 & 0 & 0 & 0 \\ (4) & 0 & 0 & 0 & 0 & 0 & 0 & 0 & 0 & 0 & 0 \\ (5) & 0 & 0 & 0 & 0 & 0 & 0 & 0 & 0 & 1 & 0 \\ (6) & 0 & 0 & 0 & 0 & 0 & 0 & 0 & 0 & -1 & 0 \\ (7) & 0 & 0 & 0 & 0 & 0 & 0 & 0 & 0 & 0 & 0 \\ (8) & 0 & 0 & 0 & 0 & 0 & 0 & 0 & 0 & 0 & 0 \\ (9) & 0 & 0 & 0 & 0 & 0 & 0 & 0 & 0 & 0 & 0 \\ (10) & 0 & 0 & 0 & 0 & 0 & 0 & 0 & 0 & 0 & 0 \end{array}$$

	(11))	(12)	(13)	(14)	(15)	(16)	(17)	(18)	(19)	(20)	(21)	(22)	(23)
(1)	$-f$	0	0	0	0	0	0	0	0	1	f	$-a$	0
(2)	f	0	0	0	0	0	0	0	0	1	$-f$	$-a$	0
(3)	0	0	0	0	-1	$-f$	0	0	0	1	f	a	0
(4)	0	0	0	0	-1	f	0	0	0	1	$-f$	a	0
(5)	b_f	0	0	0	0	0	0	0	-1	0	b_v	0	$-a$
(6)	$-b_f$	0	0	0	0	0	0	0	1	0	$-b_v$	0	a
(7)	0	0	0	1	0	b_f	0	0	-1	0	b_v	0	a
(8)	0	0	0	- 1	0	$-b_f$	0	0	1	0	$-b_v$	0	$-a$
(9)	0	0	-1	0	0	0	0	0	0	0	0	0	1
(10)	0	0	0	0	0	0	0	-1	0	0	0	0	1

(13) [cont.]

Vectors of interactions carried by the first- and second-stage suspensions are calculated form well-known formulae:

$$\mathbf{R}_p = \{\mathbf{k}_p\}\,\mathbf{u}_p + \{\mathbf{c}_p\}\,\dot{\mathbf{u}}_p\,, \qquad \mathbf{R}_s = \{\mathbf{k}_s\}\,\mathbf{u}_s + \{\mathbf{c}_s\}\,\dot{\mathbf{u}}_s\,. \tag{14}$$

The static vertical pressures of the wheels onto the rails, resulting from rail-vehicle's weight, equal

$$G = 0.5\,(0.25M_b + 0.5M_f + M_w)\;g, \tag{15}$$

while the dynamic vertical pressures of the right and the left wheel of the j-th wheel set, resulting from spatial vibrations of the vehicle, are calculated from the formulae

$$\left.\begin{aligned} P_{v1j} &= \frac{b+e}{2b}R_{p,2j-1} + \frac{b-e}{2b}R_{p,2j} \\ P_{v2j} &= \frac{b-e}{2b}R_{p,2j-1} + \frac{b+e}{2b}R_{p,2j} \end{aligned}\right\} \quad j = 1,\ 2,\ 3,\ 4. \tag{16}$$

The total vertical pressures of the wheels onto the rails, P_1 and P_2, occurring in Eqs. (5), are respective sums of the static pressure G and dynamic vertical pressures given by formulae (16). In Eqs. (4)–(6) the following expressions are to be substituted

$$v_x = \frac{\bar{v}\gamma}{r}q_{2j-1} + b\dot{q}_{2j}, \qquad v_y = \dot{q}_{2j-1} - \bar{v}q_{2j}, \tag{17}$$

while $u\,(t) = q_{2j-1}$ in Eq. (9).

The external load of the rigid bodies that create the rail-vehicle is constituted by the interactions carried by the first- and second-stage suspensions, the sliding friction forces F_{x1j}, F_{x2j}, F_{y1j}, F_{y2j} and the horizontal pressures of the rail heads onto the wheel flanges, P_{h1j}, P_{h2j}, where $j = 1, 2, 3, 4$ is a number of a wheel set.

A vector of the generalised loads of wheel sets has the final form:

$$\mathbf{R}_w = \begin{bmatrix} P_{h21} - P_{h11} - F_{y11} - F_{y21} \\ \quad -(F_{x11} + F_{x21})\ b \\ P_{h22} - P_{h12} - F_{y12} - F_{y22} \\ \quad -(F_{x12} + F_{x22})\ b \\ P_{h23} - P_{h13} - F_{y13} - F_{y23} \\ \quad -(F_{x13} + F_{x23})\ b \\ P_{h24} - P_{h14} - F_{y14} - F_{y24} \\ \quad -(F_{x14} + F_{x24})\ b \end{bmatrix}. \tag{18}$$

Forces $\mathbf{R}_p$, $\mathbf{R}_s$, $\mathbf{R}_w$ are working on displacements determined by $\mathbf{q}$. The total work of the external load equals

$$L = -\mathbf{u}_p^{\mathrm{T}}\mathbf{R}_p - \mathbf{u}_s^{\mathrm{T}}\mathbf{R}_s + \mathbf{u}_w^{\mathrm{T}}\mathbf{R}_w, \tag{19}$$

where

$$\mathbf{u}_w = \mathbf{A}_w\mathbf{q}\,, \qquad \mathbf{A}_w = [\mathbf{I}\,,\,\mathbf{0}]\,, \qquad \mathbf{I} = \mathrm{diag}\,(1, 1, ..., 1)\,, \qquad \dim \mathbf{I} = 8 \times 8\,. \tag{20}$$

Substituting formulae (12), $(20)_1$ into Eq. (19) yields the final formula

$$L = \mathbf{q}^{\mathrm{T}}\mathbf{F}, \tag{21}$$

where

$$\mathbf{F} = -\mathbf{A}_p^{\mathrm{T}}\mathbf{R}_p - \mathbf{A}_s^{\mathrm{T}}\mathbf{R}_s + \mathbf{A}_w^{\mathrm{T}}\mathbf{R}_w. \tag{22}$$

After substituting forms (10), (21) into the first-rank Lagrange's equations, one obtains matrix equation of motion of the rail-vehicle, written partly in the implicit form, i.e.

$$\mathbf{B}\ddot{\mathbf{q}} = \mathbf{F}. \tag{23}$$

Convergence of the iterative process in numerical integration of Eq. (23) can be increased via transferring linear components from vector $\mathbf{F}$ on the left side of Eq. (23). Taking into account formulae (12, 14, 22), one obtains matrix equation of motion of the moving rail-vehicle in the following final form:

$$\mathbf{B}\ddot{\mathbf{q}} + \mathbf{C}\dot{\mathbf{q}} + \mathbf{K}\mathbf{q} = \mathbf{F}\,(\mathbf{q}, \dot{\mathbf{q}})\,, \tag{24}$$

where

$$\mathbf{C} = \mathbf{A}_p^{\mathrm{T}}\,\{\mathbf{c}_p\}\,\mathbf{A}_p + \mathbf{A}_s^{T}\,\{\mathbf{c}_s\}\,\mathbf{A}_s, \qquad \mathbf{K} = \mathbf{A}_p^{\mathrm{T}}\,\{\mathbf{k}_p\}\,\mathbf{A}_p + \mathbf{A}_s^{\mathrm{T}}\,\{\mathbf{k}_s\}\,\mathbf{A}_s, \qquad \mathbf{F}\,(\mathbf{q}, \dot{\mathbf{q}}) = \mathbf{A}_w^{\mathrm{T}}\mathbf{R}_w. \tag{25}$$

Equations (24) are still partly in the implicit form. The left sides of Eq. (24) are linear. Physic non-linearity connected with snaking and lateral impacts of wheel sets is hidden in vector $\mathbf{F}$. Equations (24) govern transient and quasi-steady-state vibrations of a moving rail-vehicle. A recurrent-iterative algorithm for numerical integration of matrix equations of motion like Eq. (24), based on linear prediction of the interactions and Newmark's average acceleration method [6], has been published in Ref. [5].

Snaking of wheel sets at a given service velocity $\bar{v}$, may be asymptotically stable, stable or unstable. A snaking process can be initialised assuming non-zero initial values of the generalised velocities related to the vehicle body or/and the trucks. A large number of introductory simulations performed by the author have pointed that type of vibrations and quasi-steady-state vibrations are independent of initial conditions. Assuming only one non-zero initial velocity $v_{23} = 0.01$ rad/s results in relatively fast stabilization of the vehicle's vibrations. The initial accelerations are then equal (see Eq. (24))

$$\ddot{\mathbf{q}}(0) = -\mathbf{B}^{-1}\mathbf{C}\dot{\mathbf{q}}(0). \tag{26}$$

5. Analysis of spatial vibrations of a moving Shinkansen rail-vehicle

Taking into consideration the vibration theory of a rail-vehicle developed in this study, a computational algorithm for determining quasi-steady-state responses has been formulated and programmed in Pascal.

There is considered a repeatable rail-vehicle of Shinkansen trains [7]. Values of the parameters describing the spatial model of the rail-vehicle have been taken from Refs. [7, 8]. Part of those parameters had to be estimated since there is no literature data for them. The parameters' values assumed in this paper are collected in Table 1.

Table 1. Values of the parameters describing a spatial model of a Shinkansen rail-vehicle

parameter	unit	value	parameter	unit	value
M_w	kg	2400	c_{2v}	N s/m	21675
J_{wz}	kg m^2	1350	k_{2h}	N/m	443500
M_f	kg	4950	c_{2h}	N s/m	21675
J_{fx}	kg m^2	1950	$k_{2\varphi}$	N m/rad	1419000
J_{fy}	kg m^2	6150	$c_{2\varphi}$	N m s/rad	68800
J_{fz}	kg m^2	7900	r	m	0.50
M_b	kg	36000	a_o	m	0.015
J_{bx}	kg m^2	85700	h_o	m	0.030
J_{by}	kg m^2	1894000	η	1	1
J_{bz}	kg m^2	1800000	l_o	m	25.00
k_{1v}	N/m	1270000	$2a$	m	17.50
c_{1v}	N s/m	9815	$2c$	m	2.50
k_{1h}	N/m	1270000	$2e$	m	1.90
c_{1h}	N s/m	9815	$2f$	m	2.10
$k_{1\varphi}$	N m/rad	1435000	b_v	m	1.10
$c_{1\varphi}$	N m s/rad	11000	b_f	m	0.30
k_{2v}	N/m	443500	h_f	m	0.60

The parameters describing the rails have the following values: $2b = 1.50$ m, $\gamma = 1/40 = 0.0025$, $d = 1.5$ cm, $\mu = 0.06$. The parameters of numerical integration of Eq. (24), according to the algorithm published in Ref. [5], equal: time step $h = 0.0001$ s, smoothing parameter $\lambda = 0.01$ m/s, accuracy of iteration $\varepsilon = 0.01$ N. These values of the numerical parameters protect accuracy 0.001 mm in translations and 0.001 mrad in rotations.

The simulations have been performed for service velocities $\bar{v} = 160 - 300$ km/h. Figures 10–21 present quasi-steady-state vibrations at selected service velocities (230, 250, 270 km/h) in the form

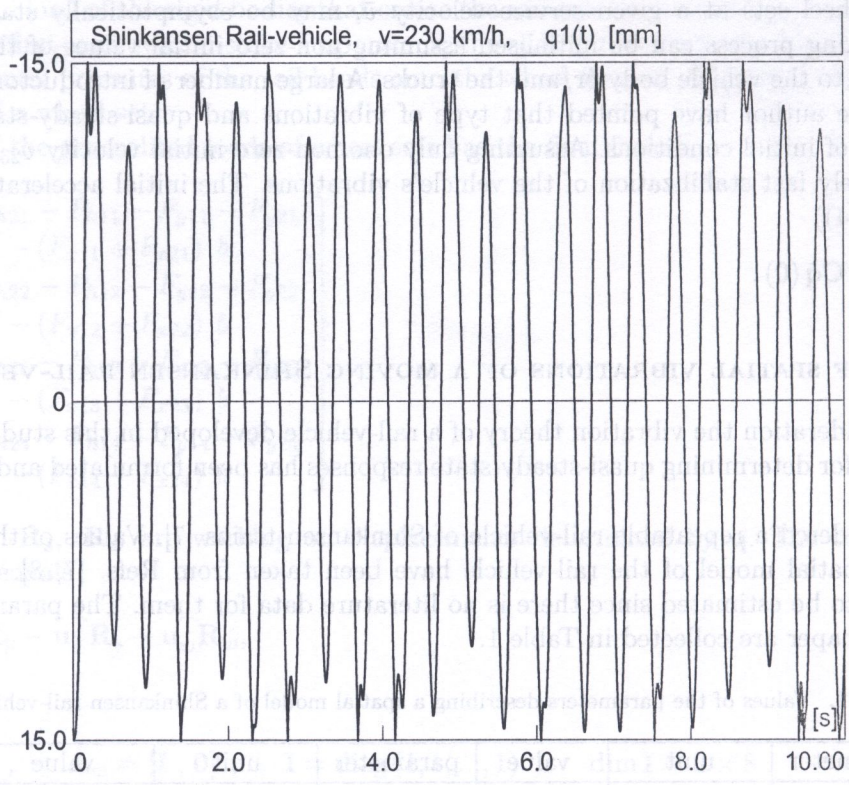

Fig. 10. Time history $q_1(t)$ of a Shinkansen rail-vehicle at service velocity 230 km/h

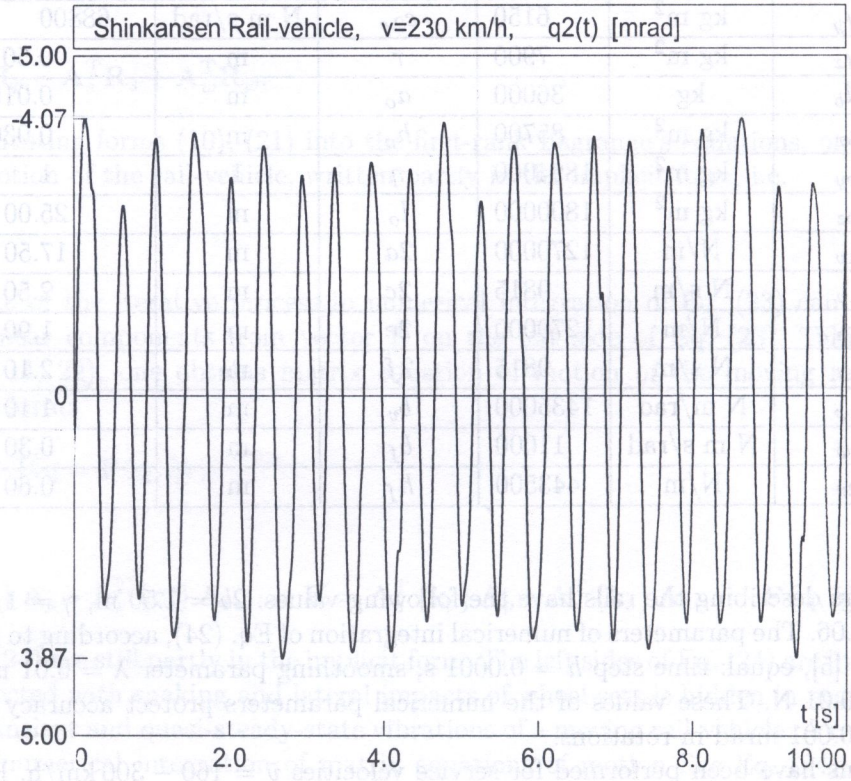

Fig. 11. Time history $q_2(t)$ of a Shinkansen rail-vehicle at service velocity 230 km/h

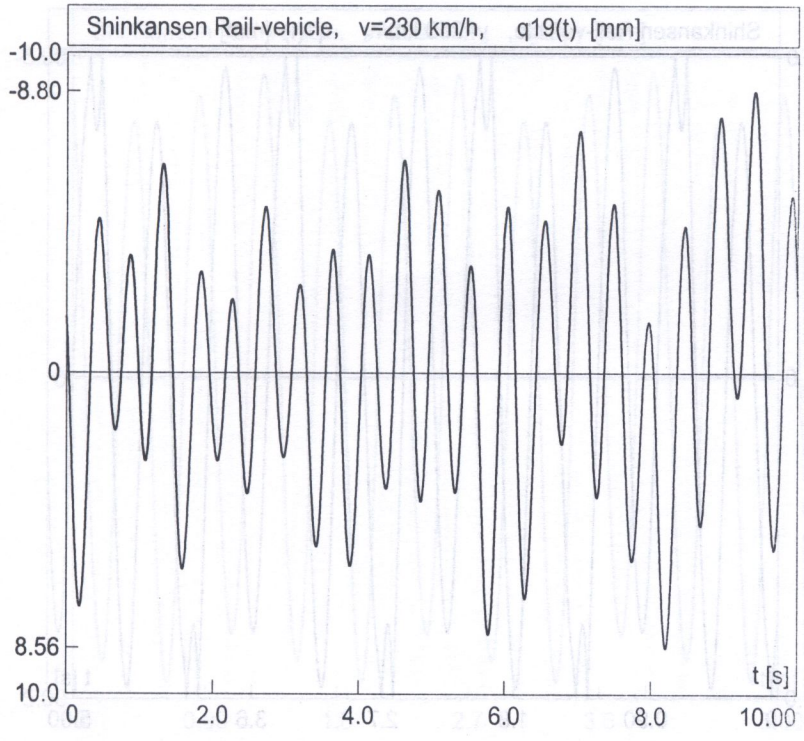

Fig. 12. Time history $q_{19}(t)$ of a Shinkansen rail-vehicle at service velocity 230 km/h

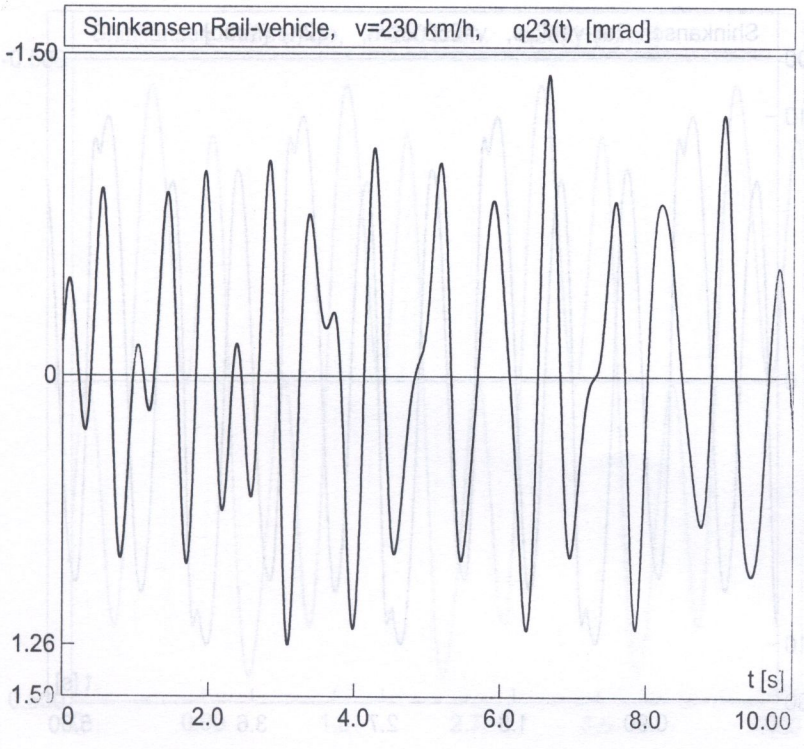

Fig. 13. Time history $q_{23}(t)$ of a Shinkansen rail-vehicle at service velocity 230 km/h

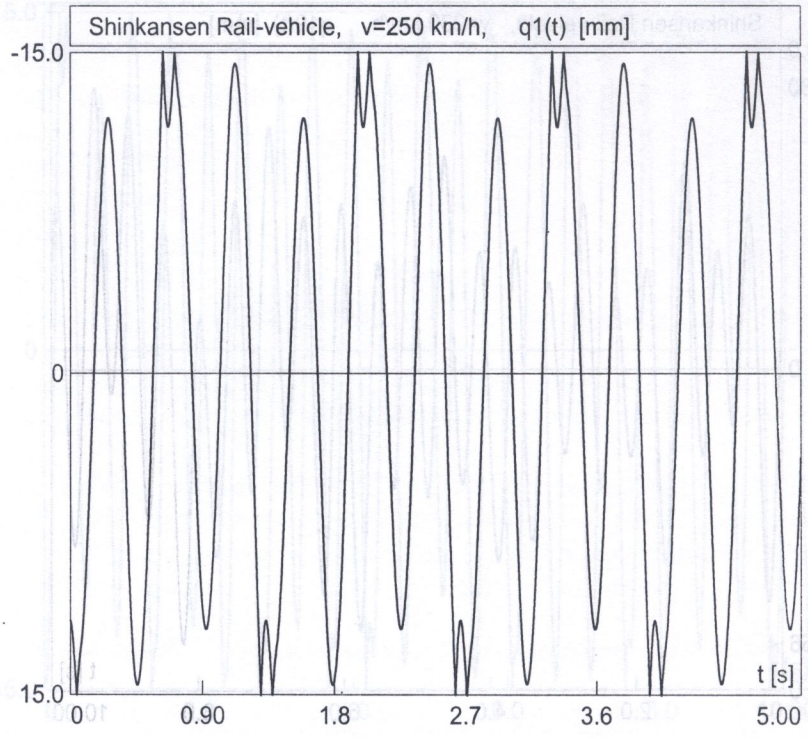

Fig. 14. Time history $q_1(t)$ of a Shinkansen rail-vehicle at service velocity 250 km/h

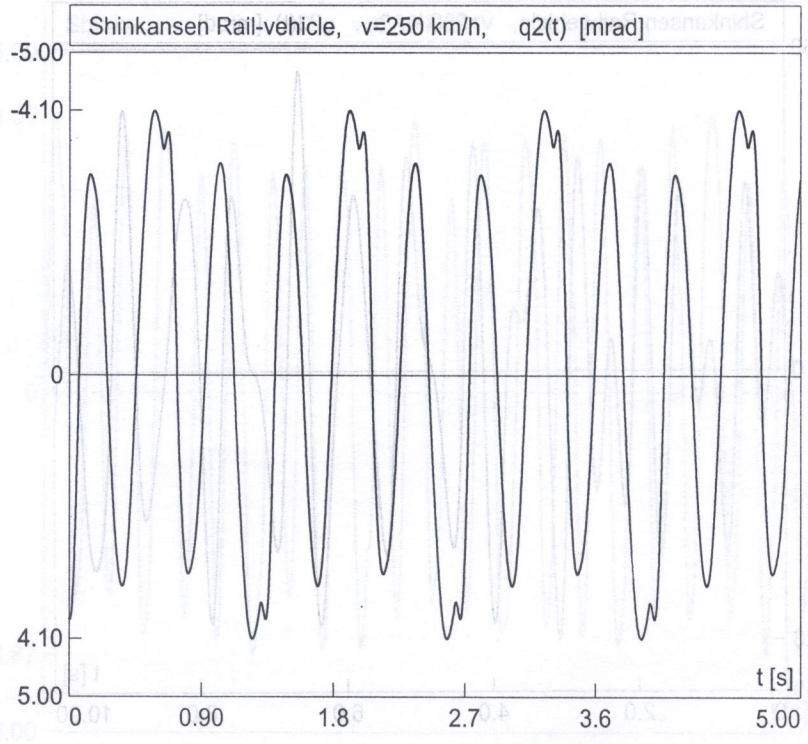

Fig. 15. Time history $q_2(t)$ of a Shinkansen rail-vehicle at service velocity 250 km/h

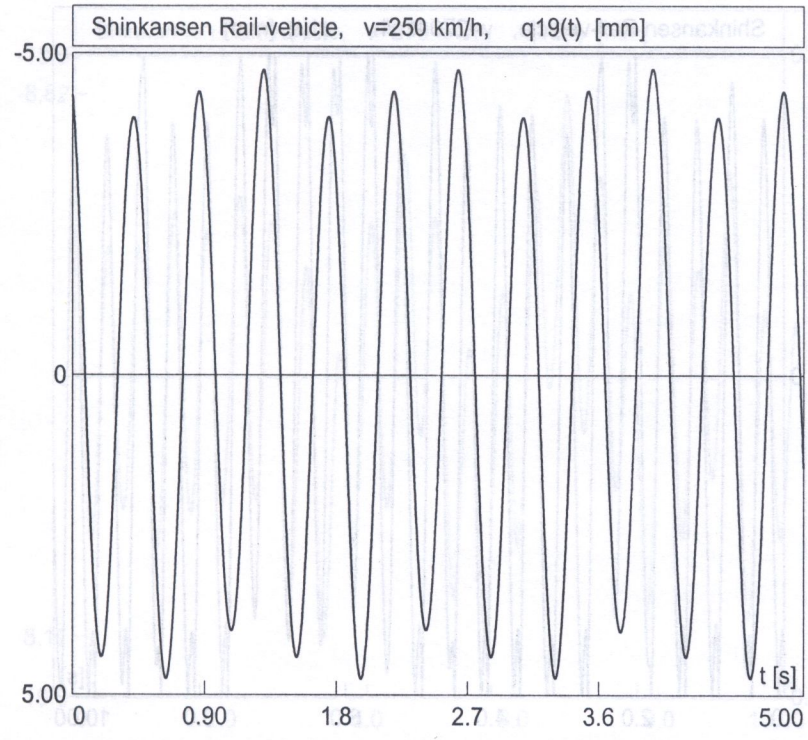

Fig. 16. Time history $q_{19}(t)$ of a Shinkansen rail-vehicle at service velocity 250 km/h

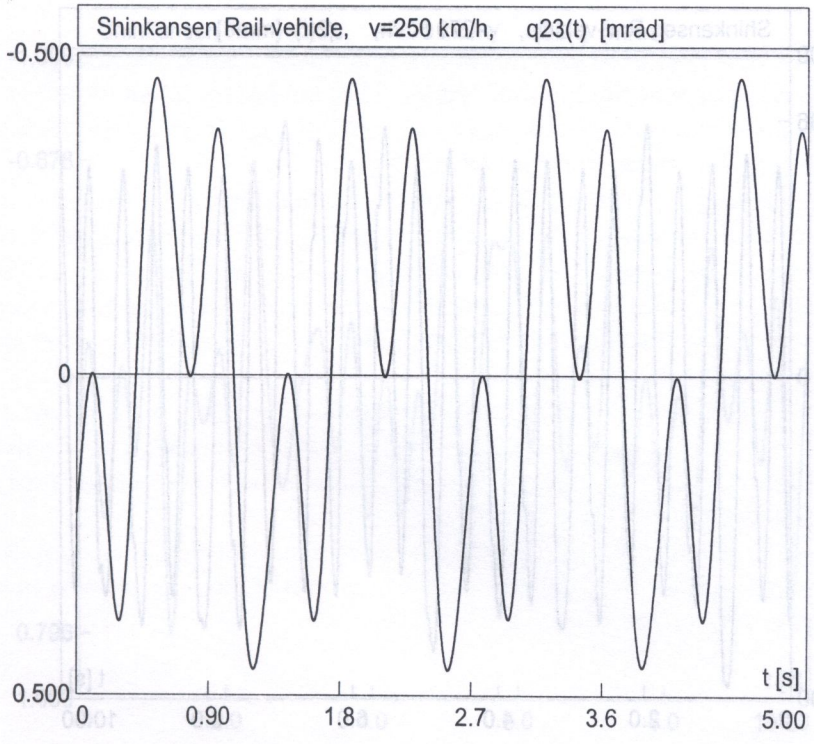

Fig. 17. Time history $q_{23}(t)$ of a Shinkansen rail-vehicle at service velocity 250 km/h

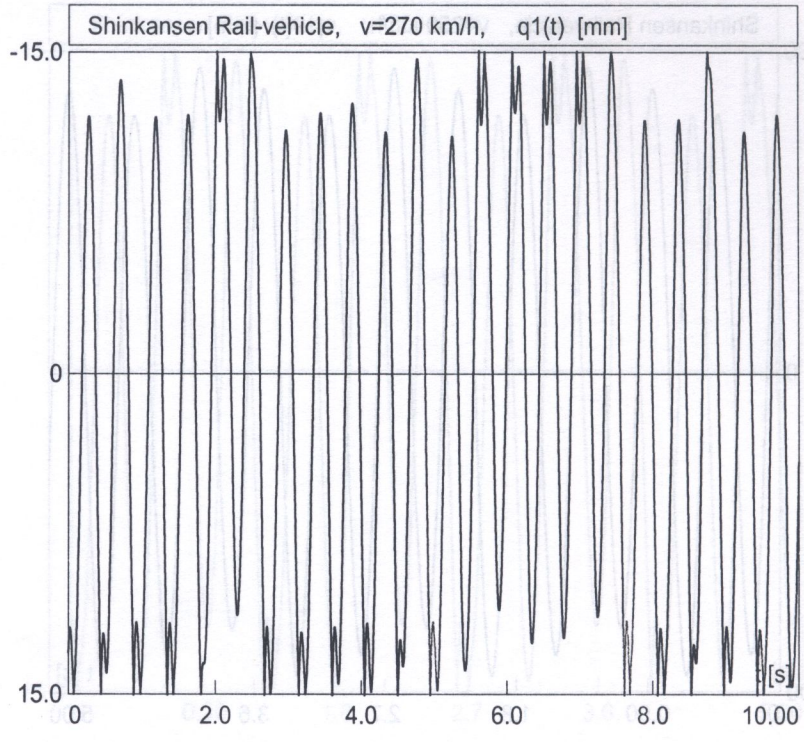

Fig. 18. Time history $q_1(t)$ of a Shinkansen rail-vehicle at service velocity 270 km/h

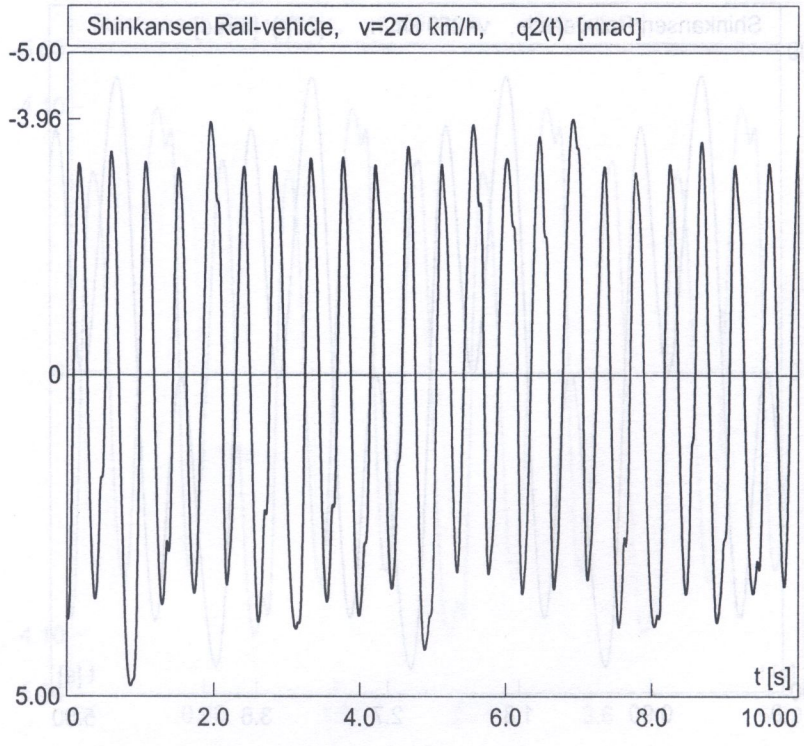

Fig. 19. Time history $q_2(t)$ of a Shinkansen rail-vehicle at service velocity 270 km/h

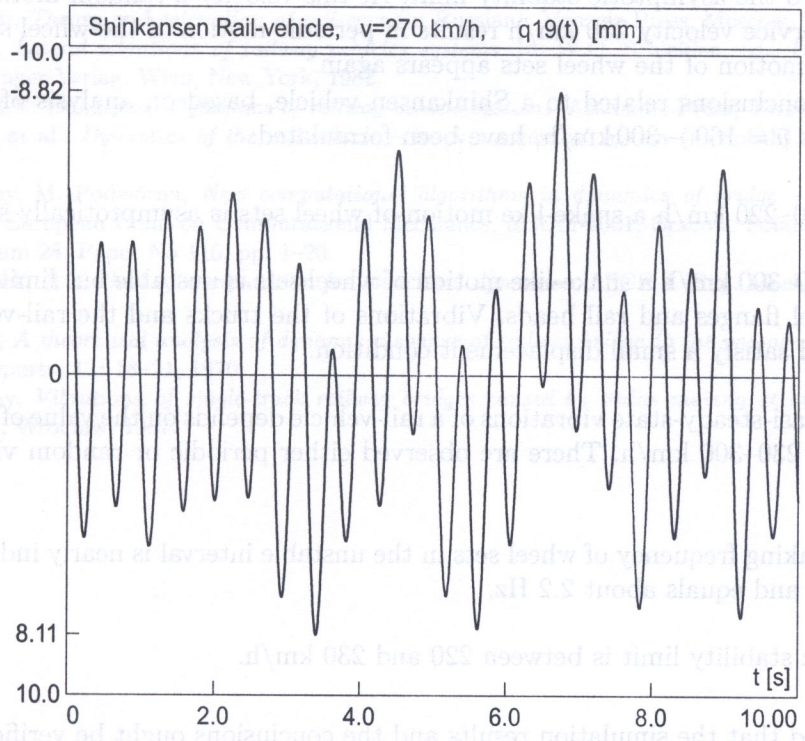

Fig. 20. Time history $q_{19}(t)$ of a Shinkansen rail-vehicle at service velocity 270 km/h

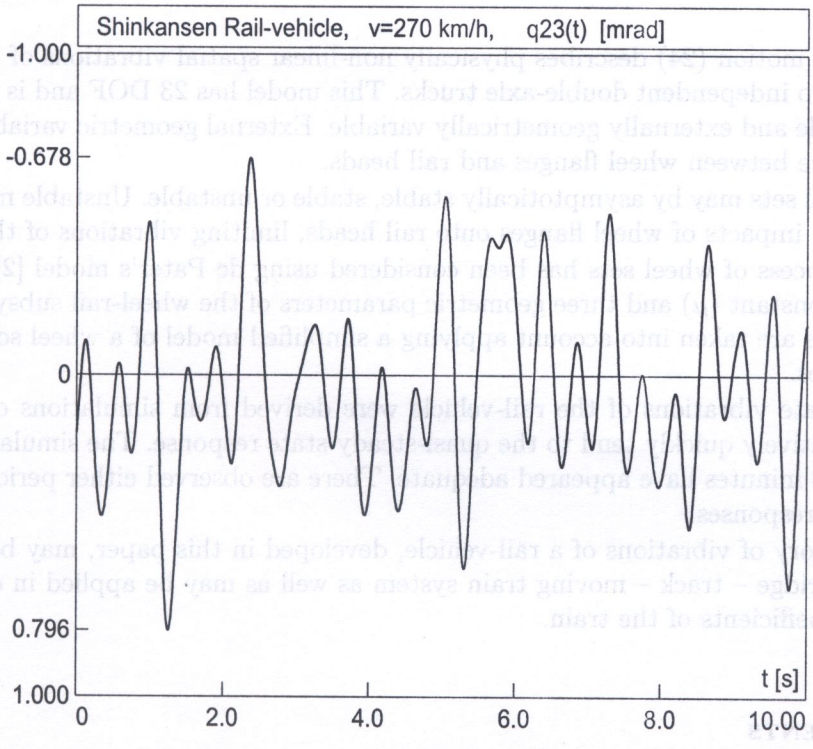

Fig. 21. Time history $q_{23}(t)$ of a Shinkansen rail-vehicle at service velocity 270 km/h

of intervals of the time histories of selected generalised coordinates of the vehicle. Service velocity 230 km/h is close to the asymptotic stability limit. At this velocity a random motion of the wheel sets is observed. Service velocity 250 km/h results in periodic motion of the wheel sets. At velocity 270 km/h random motion of the wheel sets appears again.

The following conclusions related to a Shinkansen vehicle, based on analysis of the simulation results at velocities $\bar{v} = 160 - 300\,\mathrm{km/h}$, have been formulated:

1. At velocities 160–220 km/h a snake-like motion of wheel sets is asymptotically stable.

2. At velocities 230–300 km/h a snake-like motion of wheel sets is unstable but limited by clearance d between wheel flanges and rail heads. Vibrations of the trucks and the rail-vehicle body are also limited and satisfy a small displacement condition.

3. The shape of quasi-steady-state vibrations of a rail-vehicle depends on the value of service velocity from the range 230–300 km/h. There are observed either periodic or random vibrations of the vehicle.

4. The average snaking frequency of wheel sets in the unstable interval is nearly independent of the service velocity and equals about 2.2 Hz.

5. The asymptotic stability limit is between 220 and 230 km/h.

It must be noted that the simulation results and the conclusions ought be verified for the exact values of the parameters for a Shinkansen rail-vehicle model.

6. Conclusions

Matrix equation of motion (24) describes physically non-linear spatial vibrations of the model of a rail-vehicle with two independent double-axle trucks. This model has 23 DOF and is internally geometrically invariable and externally geometrically variable. External geometric variability is limited by a finite clearance between wheel flanges and rail heads.

Snaking of wheel sets may by asymptotically stable, stable or unstable. Unstable motion of wheel sets induces lateral impacts of wheel flanges onto rail heads, limiting vibrations of the vehicle.

The snaking process of wheel sets has been considered using de Pater's model [2], described by a single material constant (μ) and three geometric parameters of the wheel-rail subsystem (b, r, γ). The lateral impacts are taken into account applying a simplified model of a wheel set with linearly elastic wheel flanges.

Quasi-steady-state vibrations of the rail-vehicle were derived from simulations of transient vibrations which relatively quickly tend to the quasi-steady-state response. The simulations in a time interval lasting 1–3 minutes have appeared adequate. There are observed either periodic or random quasi-steady-state responses.

A nonlinear theory of vibrations of a rail-vehicle, developed in this paper, may be incorporated in modelling the bridge – track – moving train system as well as may be applied in calculating the running comfort coefficients of the train.

Acknowledgments

This work has been supported by the State Committee for Scientific Research, Poland, under Grant No 8 T07E 024 20. This support is gratefully acknowledged.

References

[1] A.N. Nikolskij, *Theory and calcuation of rail-cars* (in Russian). Maszgiz Press, Moscow, 1947.

[2] A. De Pater, *Lateral vibrations of railway vehicles systems.* In: W.O. Schiehlen, ed., *Dynamics of high-speed vehicles.* Springer-Verlag, Wien; New York, 1982.

[3] V.K. Garg, R.V. Dukkipati, *Dynamics of railway vehicle systems.* Academic Press, Toronto; Tokyo, 1984.

[4] J. Kisilowski at al., *Dynamics of the rail-vehicle – track mechanical system* (in Polish). PWN Press, Warsaw, 1991.

[5] M. Klasztorny, M. Podwórna, *New computational algorithms in dynamics of bridge – track – moving train system*, 2-nd European Conf. on Computational Mechanics, ECCM-2001, Cracow, Poland, 2001, CD Proceed.: Minisymposium 28, Paper No 110, pp. 1–20.

[6] N.M. Newmark, *A method of computation for structural dynamics.* ASCE J. Eng. Mechanics Div., **85:** 67–94, 1959.

[7] A. Matsuura, *A theoretical analysis of dynamic response of railway bridge to the passage of rolling stock*, RTRI Quarterly Reports, **11**: 18–21, 1970.

[8] M. Klasztorny, *Vibrations of single-track railway bridges caused by trains moving at high speeds* (in Polish). WPWr Press, Wrocław, 1987.